



Chiral semiconductor nanorod heterostructures with high photocatalysis activity



Wei Ma^{a,b}, Jiatian Mao^{a,b}, Changlong Hao^{a,b}, Liguang Xu^{a,b,*}, Chuanlai Xu^{a,b}, Hua Kuang^{a,b}

^a State Key Lab of Food Science and Technology, Jiangnan University, Wuxi, Jiangsu, 214122, PR China

^b International Joint Research Laboratory for Biointerface and Biodetection, School of Food Science and Technology, Jiangnan University, Wuxi, Jiangsu, 214122, PR China

ARTICLE INFO

Keywords:
Semiconductor nanorods
Metal growth
Heterostructure
Circular dichroism

ABSTRACT

Chiral semiconductor nanorods and their heterostructures have attracted intense attention. In this work, it was shown that chiral amino acids on CdSe@CdS semiconductor nanorods (SNR) displayed circular dichroism bands (CD, 200–480 nm). Longer SNRs were found to induce stronger CD intensities, while an increase in the SNR diameter led to a clear CD band redshift. Multi-site post-growth of platinum (Pt) and gold (Au) further enhanced the CD intensity and induced CD band transitions. Electromagnetic calculations revealed that the metal post-growth gave rise to a strong electromagnetic field enhancement, with Pt inducing a stronger enhancement than Au. The optimized chiral multi-sites platinum on SNR displayed higher photocatalytic activities manifested that the deposited metal endowed energy transfer and enhanced the separation of photo-excited electrons and holes. These findings demonstrated that the multi-sites deposited metal provided a method to produce strong optical activity of nanostructures by adjusting the morphology of the semiconductor nanorod.

1. Introduction

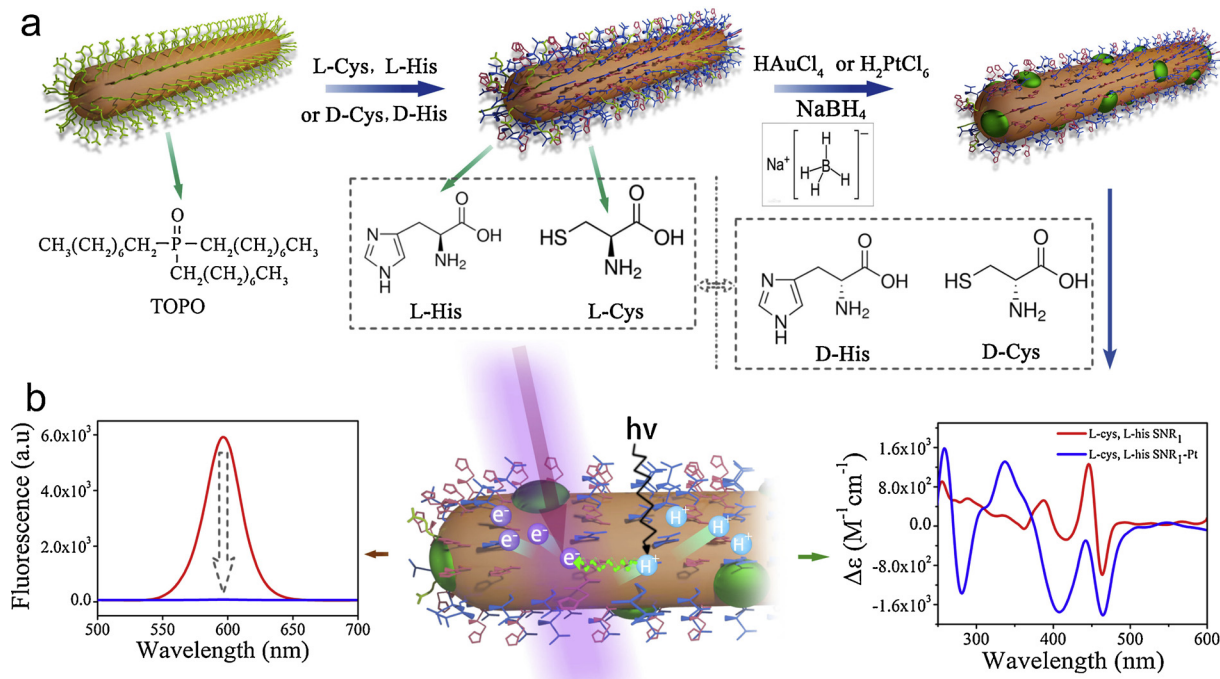
The chirality of colloidal nanocrystals (NC) [1–3] and their superstructures [4–7] have attracted significant interest in areas ranging from fundamental science to technological applications [8]. Strong chiral inorganic nanostructures not only offer new and powerful techniques for fabricating new chiral materials [9,10] and developing ultrasensitive sensors for DNA segments, small molecules, cancer antigens, and micro-ribonucleic acids [11–14] but also provide a chiroptical model for theoretical studies [15–17]. With the development of NCs synthesis and assembly techniques [18–24], several exciting chiral phenomena have been discovered, such as chiral inversion [25], chiral memory [26], and chiral coupled electron spin [27] in semiconductor NCs, and have realized that strong chirality can enable efficient applications in chiral recognition and separation [28,29], circularly polarized luminescence [30–33], chiral induced spintronic devices, and so on [34,35].

However, production of nanostructures with strong chirality still faces challenging fundamental issue. The induction of CD bands in chiral quantum dots (QDs) is difficult to interpret due to the wide size distribution of quantum dots obtained by aqueous-phase synthesis [8]. Ligand exchange with chiral amino acids for organic-phase-synthesized semiconductor nanorods (SNR) endows nanorods with better defined

characteristic bands [36–38]. Previous studies have primarily focused on the mechanism of induction of the CD, while investigations of chirality enhancement have been rare [39]. On the other hand, enantioselective fabrication of chiral NCs by postsynthetic ligand exchange provided an opportunity to investigate the applications of chiral material interactions [33]. Generally, semiconductor NCs with strong optical activity can stimulate future research into chiral fabrication for chiral materials, photovoltaics, stereoselective catalysis, and photocatalysis [40,41]. To achieve a strong chiral optical response, the postsynthetic ligand exchange strategy based on capping a chiral organic shell provides an appealing route to realize strong chiroptical characteristics coupled with the quantum size effect [42]. The diversity of amino acids provides new possibilities and strategies for producing strongly optically active semiconductor materials. New applications and potentials could be achieved, such as the electron transfer effect in nanoscale chirality coupled photoelectrochemical based water splitting [43] enabled new understanding of chirality.

Fabrication of complex architectures with a large number of components in a single structure has allowed researchers to explore combination properties [41,44,45] especially for tuning and enhancing chiroptical activity. CdSe@CdS dot-in-rod [41], CdS rods, end site doped CdS-Pt, [46,47] CdSe@CdS-Au/Pt/Pd [45,48], and multi-component hetero-nanowires (ZnS-(CdS/Au/Pt/Pd) [49,50] have been

* Corresponding authors at: State Key Lab of Food Science and Technology, International Joint Research Laboratory for Biointerface and Biodetection, PR China.
E-mail address: xuliguang2006@126.com (L. Xu).



Scheme 1. Schematic illustration of the chiral semiconductor-metal hetero-nanorod and optical properties. (a) The fabrication routes for chiral SNR Au or Pt hetero-nanorod structures. The phase transfer process replaced the organic TOPO ligand with two chiral amino acids: L-cys, L-his or D-cys, D-his. Post-growth of Au or Pt occurred at multiple sites on the semiconductor nanorods, forming multiple semiconductor-metal interface. (b) Schematic demonstration of the fluorescence and CD spectrum transitions for L-cys, L-his SNR₁ and L-cys, L-his SNR₁-Pt. The plasmonic metal post-growth induced fluorescence quenching and CD band induction and enhancement.

reported, but their applications have been limited to studies of photocatalysis [51–53]. The plasmonic effect not only helps to tune the electronic structure of SNR and induces fast electron transfer and separation [54] but also induces an optical enhancement, especially for chiroptical tuning and enhancement; however, this research direction has not been investigated to date.

Here, the strong chiral optical response of CdSe@CdS SNR was studied according to phase transfer mediated by two amino acids (cysteine and histidine), which was further enhanced by the post growth of a metal (Au, Pt) (Scheme 1a, b). The CD intensity and band position were found to be dependent on the length and diameter of the SNR, respectively. Based on the two amino acid post-synthetic ligand exchange strategy and post-metal growth, the optical activity of SNR heterostructures was strongly enhanced (*g*-factor: 2.2×10^{-3}). The results exhibited that the combination of a semiconductor and multi-sites metal heterostructures was able to be used to fabricate a strong optical active system. The energy band was adjusted by multi-sites metal deposition, and induced fluorescence quenching effects and high photocatalysis activity.

2. Results and discussion

2.1. Fabrication of chiral semiconductor nanorod

Wurtzite CdSe and CdSe@CdS SNR were synthesized in trioctylphosphine oxide (TOPO) using the classical hot-injection technique with slight modification [55,56]. The amounts of the CdSe seed, octadecylphosphonic acid (ODPA), and hexylphosphonic acid (HPA) were optimized to control the aspect ratio (AR). The prepared SNR (CdSe, CdSe@CdS) samples were good dispersed with a well-grown rod shape and displayed a typical band edge transition of semiconductor NCs (Figs. 1a–d and S1, S2). After several centrifugation steps and dispersal in polar and nonpolar solvents, the final SNR was suspended in chloroform. Subsequent ligand exchange with L-cys or D-cys allowed the

SNR to transfer into water without destroying the rod geometry, with good dispersity (Figs. 1a–d, S3). The energy dispersive spectrometry (EDS) results of the phase-transferred CdSe@CdS SNR showed typical Cd, S, and Se elemental peaks (Fig. S4). This work used one CdSe nanorod (length: 36.8 nm, diameter: 20.4 nm; Fig. 1a,b) and three CdSe@CdS nanorods (SNR₁, SNR₂, and SNR₃, Figs. S1 and S2), distinguished by AR, to study the chiroptical effects. Calculations of the AR for CdSe and CdSe@CdS were performed by measuring 100 individual rods, and the AR values were found to be 1.8 (CdSe), 7.2 (SNR₁), 3.6 (SNR₂), and 3.1 (SNR₃).

The CD spectra of both CdSe and CdSe@CdS (SNR₁) displayed CD bands at 350–600 nm and 250–480 nm (Fig. 1e, f), in good agreement with the UV – vis absorption spectra (Figs. S5 a–d). In particular, the CD bands for CdSe were located at 375, 446, 508, 539, and 558 nm, with the strongest CD signal at 558 nm ($20.7 \text{ M}^{-1} \text{ cm}^{-1}$). In the CD spectrum of CdSe@CdS (SNR₁), chiroptical bands were observed at 281, 326, 375, 414, 445, and 461 nm. Despite the strong CD band at 281 nm, the strongest CD signal was observed at 445 nm ($364.5 \text{ M}^{-1} \text{ cm}^{-1}$). SNR capped by chiral D-cys or L-cys displayed mirror-image spectra (+/– Cotton effect) originating from the electronic transition of the chiral ligands and excitonic transition of the SNR from the UV to visible spectra [36,57].

The complicated energy bands of a semiconductor under strong quantum confinement [58] give rise to multiple peaks in the CD spectrum for the stronger signals at 539–558 nm or for the 445–461 nm bands in the shorter wavelength region. The anisotropy factor (*g*-factor) for CdSe@CdS SNR₁ (5.2×10^{-4}) was much larger than that for CdSe nanorods (7.9×10^{-5} , Figs. S6, S7) because CdSe nanorods (AR = 1.8) were already close to their maximum *g*-factor [36]. Notably, the aqueous phase of the chiral SNR displayed strong fluorescent signals (Figs. S5e, S5f) without a quenching effect from capped chiral molecules (D or L-cysteine).

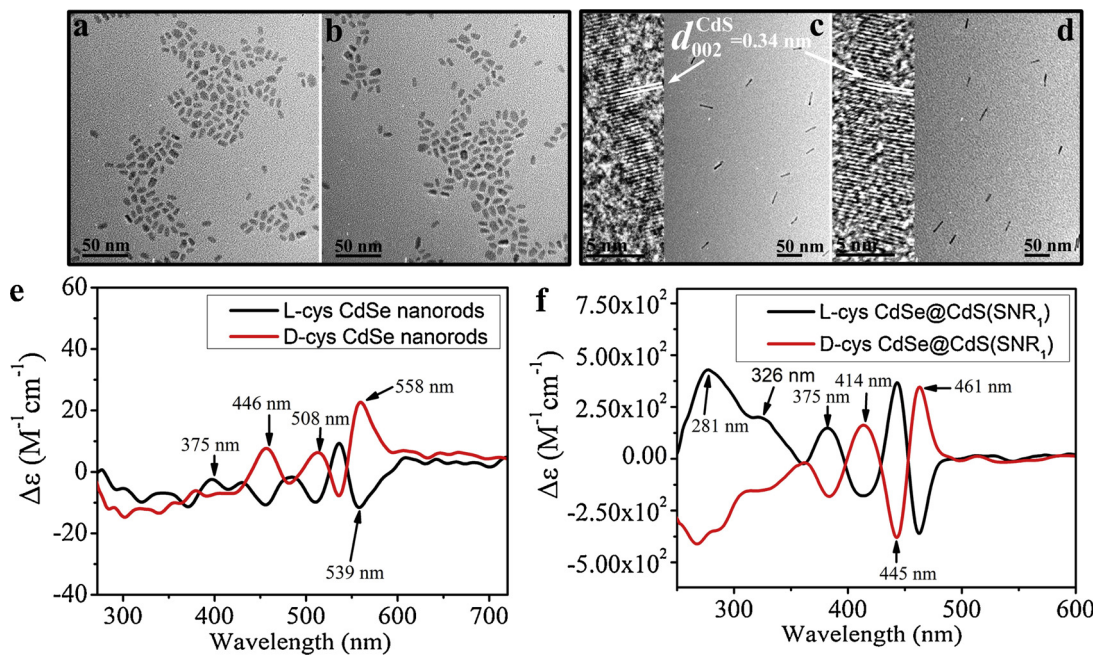


Fig. 1. (a, b) TEM of D-cys CdSe nanorods (a) and L-cys CdSe nanorods with an AR of 1.8. (b); (c, d) TEM images of D-cys CdSe@CdS nanorods (SNR₁) (c) and L-cys CdSe@CdS nanorods (SNR₁) with an AR of 7.2 (d); the corresponding HRTEM is shown as the inset; (e, f) CD spectra of D-cys/L-cys CdSe nanorods (e); and CD spectra of D-cys/L-cys CdSe@CdS nanorods (f) in which the characteristic chiral bands are labeled in each figure.

2.2. Amino acids induced a chiroptical enhancement

Since CdSe@CdS had a stronger CD intensity and larger g-factor for nanorods, we focused on the three CdSe@CdS nanorods, namely, SNR₁, SNR₂, and SNR₃, in subsequent experiments. To improve SNR phase transfer from chloroform into water, we employed combinations of D-cys, D-his or L-cys, L-his for SNR₁, SNR₂, and SNR₃. The CD intensity was much stronger than that for single Cys (D-cys or L-cys only) phase transferred nanorods (Figs. 2a–c, 1f), and the SNR were dispersed well with the rod geometry (Fig. S8). The SNR chirality can originate from:

- 1) Possible intrinsic chiral SNR, called inorganic L-chiral and D-chiral enantiomers arising from defects, e.g., screw and edge dislocations and interstitial point defects, or atoms;
- 2) Chiral surfaces consisting of chiral molecules and achiral SNR that induce an electronic transition between the chiral ligands and SNR.

The first chiral mechanism is theoretically possible and has been reported in CdSe@ZnS nanorods [37,59]. We further investigated the CD spectra both in water and for residues in hexane extracted from chloroform and found the same type of chirality when using D-cys, D-his for the phase transfer (Fig. S9). High-resolution transmission electron microscopy (HRTEM) showed that the CdS (002) crystals lattice had regular crystals edges (Figs. 1c, d, 2d–f). We assumed that the chirality was due to the binding of chiral amino acids. The same type of chirality from D-cys, D-his SNR₁ was due to the very small amount of amino acids that transferred into chloroform and hexane.

The second proposed chiral mechanism involves the adsorption of chiral amino acids on the surface of semiconductor NCs [25,33,36] and can include a) the electronic hybridization of chiral ligands and SNR by dipole–dipole interactions [33], and b) a geometrical arrangement of the chiral ligands on the NC surface [25,33,60]. We attributed our observed CD results to the hybridization of the achiral SNR and chiral ligand electronic states because the chiral molecules adsorbed on the NC surface destroyed the intrinsic symmetry of SNR and induced optical activity. To investigate the binding effect of chiral ligands on the SNR surface, we performed DOSY NMR measurements. The NMR spectrum revealed that the D-cys- (or L-cys)-functionalized SNR induced

an up-field shift to 3.56 ppm that was due to the binding of thiol groups to Cd surface atoms (Figs. S10 and S11). The signals of the amino acid molecules (D-cys) corresponded to diffusion coefficients of $1.06 \times 10^{-9} \text{ m}^2/\text{s}$ (Peak 1: 3.89 ppm, Table S1), which were higher than the diffusion coefficient of D-cys SNR (7.47×10^{-10} , peak 1, 3.56 ppm, Table S2). These result indicated that the ligands diffused together with the semiconductor nanorods. This could be the reason for splitting of peak 3 and peak 4 (Figure S11). When SNR₁ was phase transferred by D-penicillamine or L-penicillamine, the chiroptical bands were similar to those of the SNR that was phase-transferred by chiral D-cys or L-cys (Fig. S12). This result reflects the similar chiral centers in penicillamine and cysteine that form similar chiral surfaces on SNR when their thiol groups are anchored to Cd atoms.

When D-his or L-his alone was used for the phase transfer, the obtained CD spectra displayed characteristic bands at the first absorbance peak at approximately 450 nm (Fig. S13). Binding via thiol and COO⁻ groups was able to densely bind molecules on the surface of the QDs and hence induce chirality [25,60]. For the present case of histidine-assisted SNR phase transfer, the carboxyl group (from histidine) bonded to surface Cd atoms in carboxylate form. The hydrogen chemical shift of 3.88 ppm was up-field shifted to 3.50 ppm in the ¹H NMR spectra (peak 4, see Tables S3 and S4). The peak 1, and peak 2 was not chemical shifted demonstrating weak interaction with CdS surface. The diffusion coefficients of free D-his were higher than the diffusion coefficient of D-his SNR, indicating that the ligands diffused together with the semiconductor nanorods. (Figs. S14 and S15). Since the different diffusion coefficients had the same order of magnitude, the D-his should be anchored to the surface through single point binding with the other part of D-his, similar (on the surface) to free D-his. The free D-his was removed by dialysis which can be seen from NMR data (Figs. S15 and S16). We also found that the dialysis did not affect the chemical shift and shape of D-his (Figs. S14 and S17). The concentration of amino acids was approximately the same for all of the NMR spectra, excluding the interference [61]. We proposed that the carboxyl groups were bonded to the Cd atoms on the SNR surface while the S atoms were negatively charged. The binding-induced chemical shift was normal for histidine [62], while the shape of the proton signals was not changed in our study. The binding of the two amino acids (cysteine and histidine)

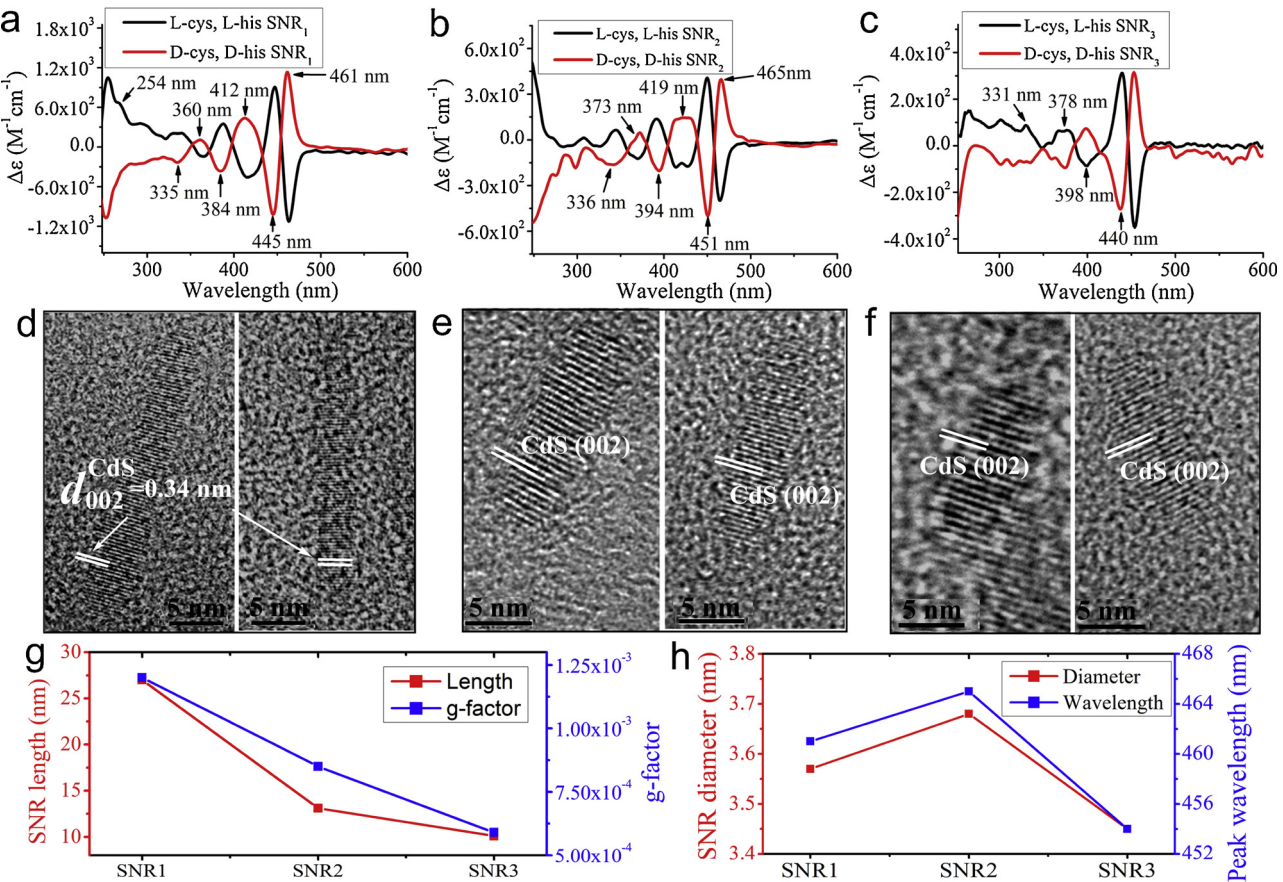


Fig. 2. (a–c) CD spectra of the d-cys, d-his (and l-cys, l-his) two amino acid phase transferred SNR₁ (AR: 7.2) (a), SNR₂ (AR: 3.6) (b) and SNR₃ (AR: 3.1) (c); (d–f) HRTEM for the d-cys, d-his SNR₁ (left) and l-cys, l-his SNR₁ (right) (d); (e) d-cys, d-his SNR₂ (left) and l-cys, l-his SNR₂ (right); (f) d-cys, d-his SNR₃ (left) and l-cys, l-his SNR₃ (right); the CdS (002) crystals lattice is labeled in each TEM image; (g, h) the g-factor (g) and peak wavelength (h) plotted against the length and diameter of SNR₁, SNR₂, and SNR₃, which are related to the electronic hybridization effect.

can help to enhance the CD intensity (Figs. 1f and 2 a). The CD signal of d-cys, d-his (or l-cys, l-his) SNR was due to the hybridization of the achiral SNR and chiral ligand electronic states, while the two amino acids gave rise to a strong enhancement of the chiral optical response.

2.3. Chiroptical properties

The SNR did not display any chiroptical bands when racemic cysteine and histidine mixtures (D, L-cys, D, L-his) were used for the phase transfer (Fig. S18) mainly because the racemic mixture of L-Cys and D-cys eliminated the overall chirality at the semiconductor interface. Distinct from CdSe QDs [60], non-thiol chiral ligands, e.g., tartaric acid or a combination with an achiral thiol ligand (3-mercaptopropionic acid, MPA) used for phase transfer, failed to induce CD bands, with only the band from tartaric acid observed at 240 nm (Fig. S19). The SNR₁ phase-transferred by two amino acids (cysteine and histidine) displayed stronger CD bands than the single cysteine-phase-transferred SNR₁, with the bands in the 200–350 nm range, while CdSe exhibited weak CD bands in this region (Fig. S20).

Removal of free d-cys and d-his by dialysis did not significantly reduce the CD intensity, indicating that the strongly bound amino acid(s) were the source of the chirality (Fig. S8). In this study, the combination of d-cys, d-his (or l-cys, l-his) induced a stronger CD intensity (Figs. 1f and 2 a), while SNR remained highly luminescent (Figs. S21 and S22). Longer SNR rods induced stronger CD intensities (461 nm, 1120.1 M⁻¹ cm⁻¹, Fig. 2g) and larger g-factors (SNR₁: 1.2 × 10⁻³; SNR₂: 8.4 × 10⁻⁴; SNR₃: 5.9 × 10⁻⁴), which are equivalent to the correlation between the AR and CD band intensity (Fig. S23). The increase in the CD intensity with increasing AR was due to the array of the Cd-S bonds

or carboxyl group binding in the direction of the long axis of the SNR. At the same SNR concentrations, the total number of cysteine and histidine molecules was increased (Tables S4 and S5), and the increased amino acid binding and coupling for the longer SNR gave rise to a stronger CD intensity. A larger NC diameter induced a redshift of 11 nm for chiroptical bands (Fig. 2h). This redshift may be due to the effect of the larger dimension of the SNR that have larger diameter. The results also showed that the SNR₁ phase-transferred with two amino acids had a higher g-factor value (1.2 × 10⁻³) than that of the single d-cys or l-cys SNR₁ (5.2 × 10⁻⁴; Fig. S24); this could be employed as an efficient chiral construction strategy for organic-phase-synthesized nanomaterials.

2.4. Metal-semiconductor heterostructures

Chiral d-cys, d-his- or l-cys, l-his SNR₁ was used for the post-growth of Pt and Au to investigate the CD enhancement and transition effects. Selective growth of Au or Pt on d-cys, d-his- or l-cys, l-his SNR₁ occurred at multi-sites on the CdS layer (Fig. 3a, b), in which free Pt and Au ions were removed by dialysis. The strongest CD intensity band (461 nm) was enhanced from 1120.1 to 1413.7 M⁻¹ cm⁻¹, while other chiroptical bands (443, 412, 384, and 330 nm) maintained intensities that were similar to those of the original SNR₁ (Figs. 3e and S25). The CD intensities of the chiroptical bands at 228, 255, and 281 nm were amplified and distinguishable due to the Au NCs on SNR₁, which were also characterized by UV – vis absorption, X-ray photoelectron spectroscopy (XPS) and HRTEM (Figs. S26–S29). Pt post-growth on SNR₁ was observed at multiple sites on the SNR₁ side and end and strongly induced the transition of the absorption spectra (Figs. 3b and S30).

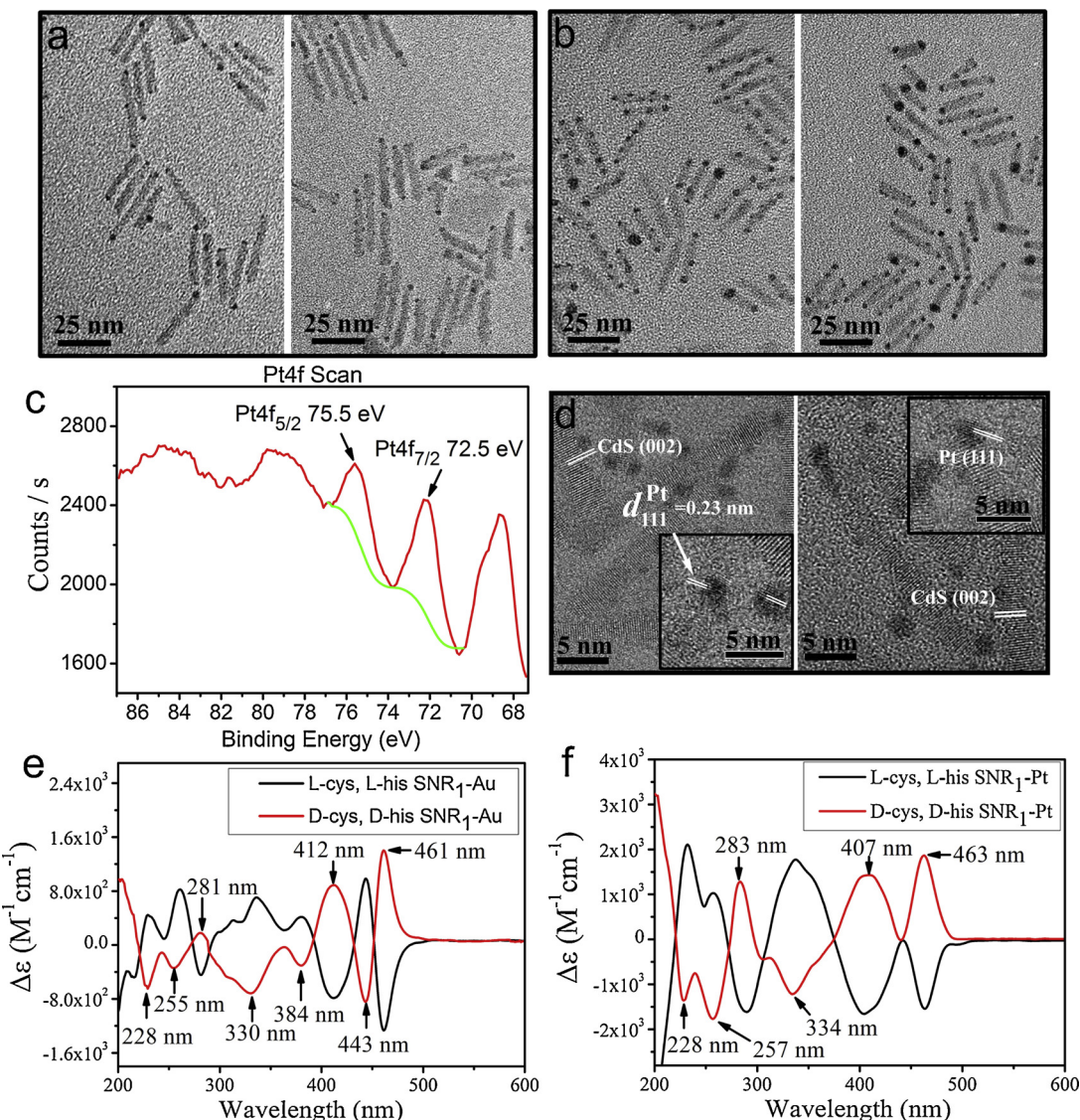


Fig. 3. (a) TEM of the d-cys, d-his SNR₁-Au hetero-nanorods (left), L-cys, L-his SNR₁-Au hetero-nanorods (right); (b) TEM of the d-cys, d-his SNR₁-Pt₂ hetero-nanorods (left) and L-cys, L-his SNR₁-Pt₂ hetero-nanorods (right); (c) XPS spectra of d-cys, d-his SNR₁-Pt₂. The arrows indicate the characteristic peaks of 72.5 eV (Pt 4f_{7/2}) and 75.5 eV (Pt 4f_{5/2}) of the heterostructures; (d) HRTEM for d-cys, d-his SNR₁-Pt₂ (left panel) and L-cys, L-his SNR₁-Pt₂ (right panel). The arrows indicate the CdS (002) and Pt (111) crystal lattices in the heterostructures; (e) CD spectra of d-cys, d-his- and L-cys, L-his SNR₁-Au hetero-nanorods; (f) CD spectra of d-cys, d-his- and L-cys, L-his SNR₁-Pt₂ hetero-nanorods.

After removing free Pt ions by dialysis, XPS showed characteristic peaks at 72.5 eV (Pt 4f_{7/2}) and 75.5 eV (Pt 4f_{5/2}) (Figs. 3c, S31 and S32), while the lattice structures of CdS (002) and Pt (111) were clearly visible in HRTEM (Fig. 3d). Pt post-growth on SNR₁ enhanced many bands (463, 407, 334, 283, 257, and 228 nm) (Figs. 3f, S33, S36) as well as suppressed the bands at 445 and 384 nm. Specifically, the CD intensity for the 461–463 nm band was enhanced from 1120.1 to 1858.5 M⁻¹ cm⁻¹, and the bands at 407–412 and 334–335 nm showed a large enhancement (454.5 to 1525.5 M⁻¹ cm⁻¹, and 229.5 to 1404.1 M⁻¹ cm⁻¹, respectively) (Fig. 3f). The band variations were due to the Pt post-growth on SNR₁ by adjusting the semiconductor energy band structure under a strong quantum confinement. The g-factors for d-cys, d-his SNR₁-Au (1.7×10^{-3}) and d-cys, d-his SNR₁-Pt (2.2×10^{-3}) were larger than that for the initial SNR₁ (Figs. S34 and S35) due to the metal-enhanced hybridization of the electronic states of the chiral ligand and achiral SNR [36]. The time kinetic CD spectra showed that CD was enhanced when the Pt content was 2.4% and 5.2%, while 8.1% Pt reduced the CD intensity (Fig. S36). Based on statistical analysis, it was found that the 2.1 nm Pt (8.1%) on SNR₁ induced the strongest CD

signals. The size of metal Pt was crucial for enhancing hybridization of the electronic states of the chiral ligand and achiral SNR. The high content of Pt may destroy the binding of amino acids on SNR surface and induce release of them during the growth process, while lower content can't induce maximum enhancement.

Au or Pt post-growth on SNR₁ was confirmed by scanning transmission electron microscopy (STEM) and EDX mapping for Cd, S, and Pt in selected areas (Fig. 4a–c). The results demonstrated that Pt and Au showed multi-site growth on the SNR. After Pt post-growth, the CD intensity for the band at 407 nm was enhanced by 3.4 times. We further calculated the electromagnetic field enhancement and found that Pt and Au induced a strong enhancement compared to the semiconductor nanorods (Figs. 4e, S37). The metal-induced CD enhancement was due to the strong surface electromagnetic fields that originated from the plasmonic metal in the hybrid semiconductor and noble metal system [63,64]. As expected, hetero-nanorod fluorescence (Fig. 4d) was completely quenched in the presence of multi-site Au or Pt, suggesting a strong energy transfer effect with enhanced charge transfer and separation in the excited state. Metal components helped to induce the

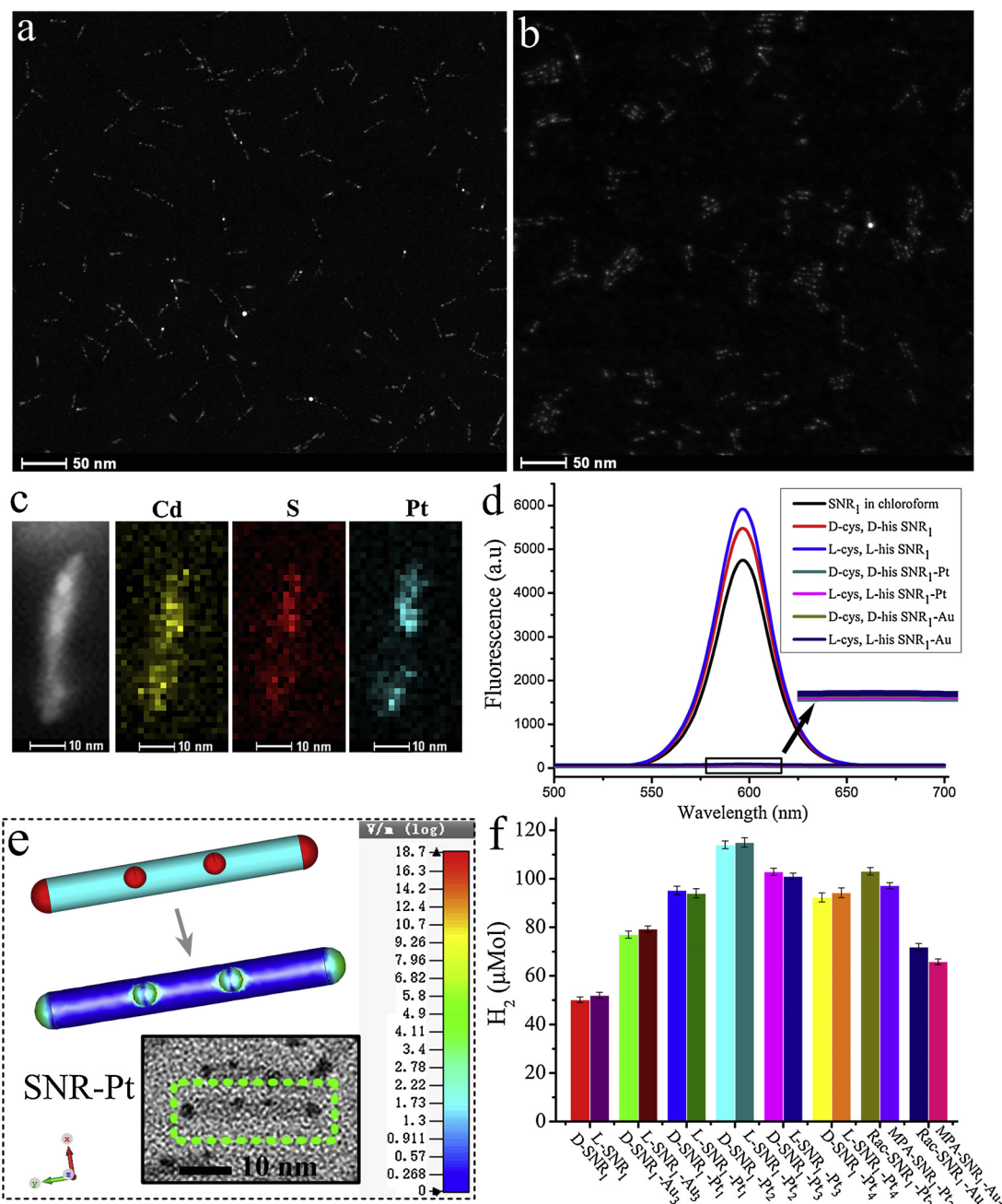


Fig. 4. (a, b) STEM images for d-cys, d-his-SNR₁-Au₃ (a) or d-cys, d-his-SNR₁-Pt₂ (b); (c) drift-corrected image for the EDX mapping of Cd, S, Pt for d-cys, d-his SNR₁-Pt₂. (d) The fluorescence spectrum for SNR in chloroform, phase-transferred d-cys, d-his SNR₁, L-cys, L-his SNR₁ and the racemic cys, his SNR₁-Au/Pt (Rac-SNR₁-Pt or Au) in water. (e) Electromagnetic field for semiconductor nanorods-metal heterostructures (SNR-Pt). (f) Photocatalysis studies based on d-cys, d-his- or L-cys, L-his SNR₁; d-cys, d-his-, or L-cys, L-his SNR₁-Au/Pt hetero-nanorods and the Rac-SNR₁-Pt₂, MPA-SNR₁-Pt₂ or Au₃ illuminated by LP light.

separation between the electrons in Pt NCs and holes in the SNR [65]. The experimental results revealed that the strong chirality of the SNR was further promoted by the electromagnetic enhancement due to the noble metal (Figs. 2a, 3 f, 4 e and S37). Electron transfer through chiral semiconductor-metal nanorods enables new future applications, such as photocatalysis. As a proof-of-concept demonstration, linearly polarized light induced photocatalytic water splitting under optimized condition (Figs. 4f, S38) indicating that H₂ production activity were in the order SNR₁-Pt₂ (5.2 wt% Pt) > SNR₁-Pt₃ (8.1 wt% Pt) > SNR₁-Pt₁ (2.4 wt% Pt) > SNR₁-Pt₄ (11.2 wt% Pt) > SNR₁-Au (2.5 wt% Au) > bare SNR₁. Different with previous metal growth on end site [65], the large areas of SNR side surface provides many active sites for promotion of catalysis activities. After growth of metal, the bandgap is reduced and

conduction band edges are decreased which is beneficial to excite electrons [49]. The semiconductor-metal hetero-nanostructures are more likely to transport photo-excited electrons from the CdS to the metallic surface, rather than remaining on the CdS surface, and holes is tend to remain on the CdS surface [66]. The electron and hole separation is particularly enhanced. The noble metal acts as an electron sink, has higher storage capacity that induced the fluorescence quenching effect. The bigger size of Pt components decreased the catalysis activities that could be due to the surface block effect for SNR. The energy band variation after metal growth potentially provide certain effect for inducing CD band transitions. Compared to racemic L-Cys and d-cys, or achiral MPA stabilized SNR-Pt or Au, the electrons transferred through chiral semiconductor-metal nanorods help to

enhance the photocatalysis activity. It was proposed that the chirality coupled in spin of electrons transferred through chiral molecules is the origin of a more efficient H₂ evolution process. The Plasmon-induced charge-carrier generation increases the concentration of electrons (and holes) reaching the surface of SNR to drive H₂ evolution.

3. Conclusion

A facile strategy to develop strong chiral semiconductor-metal hetero-nanorods was successfully established. The hetero-nanostructures obtained based on the strategy of using two amino acids, chiral ligand exchange, and post-growth provided fresh insights into plasmonic-metal-enhanced electromagnetic enhancement and the metal-enhanced chiral optical response. The proposed system enabled intense optical activity and produced energy-band-related chirality tuning. This work will open new routes for designing hybrid systems for light- and chirality-based photovoltaics, spintronics, and other applications.

Conflict of interest

The authors declare no conflict of interest.

Acknowledgment

This work was financially supported by National Key R&D Program (2017YFA0206902), and the National Natural Science Foundation of China (21631005, 21673104, 21874058, 51802125, 21771090, 31771084).

Appendix A. Supplementary data

Supplementary material related to this article can be found, in the online version, at doi:<https://doi.org/10.1016/j.apcatb.2019.01.038>.

References

- [1] A. Ben-Moshe, S.G. Wolf, M.B. Sadan, L. Houben, Z. Fan, A.O. Govorov, G. Markovich, *Nat. Commun.* 5 (2014) 4302.
- [2] A. Ben-Moshe, A.O. Govorov, G. Markovich, *Angew. Chem. Int. Ed.* 52 (2013) 1275–1279.
- [3] C. Zeng, Y. Chen, C. Liu, K. Nobusada, N.L. Rosi, R. Jin, *Sci. Adv.* 1 (2015) e1500425.
- [4] X. Lan, Z. Chen, G. Dai, X. Lu, W. Ni, Q. Wang, *J. Am. Chem. Soc.* 135 (2013) 11441–11444.
- [5] X. Lan, X. Lu, C. Shen, Y. Ke, W. Ni, Q. Wang, *J. Am. Chem. Soc.* 137 (2015) 457–462.
- [6] A. Kuzyk, R. Schreiber, H. Zhang, A.O. Govorov, T. Liedl, N. Liu, *Nat. Mater.* 13 (2014) 862–866.
- [7] A. Kuzyk, M.J. Urban, A. Idili, F. Ricci, N. Liu, *Sci. Adv.* 3 (2017) e1602803.
- [8] W. Ma, L. Xu, A.F. de Moura, X. Wu, H. Kuang, C. Xu, N.A. Kotov, *Chem. Rev.* 117 (2017) 8041–8093.
- [9] A. Kuzyk, R. Schreiber, H. Zhang, A.O. Govorov, T. Liedl, N. Liu, *Nat. Mater.* 13 (2014) 0862–0866.
- [10] W. Feng, J.-Y. Kim, X. Wang, H.A. Calcaterra, Z. Qu, L. Meshi, N.A. Kotov, *Sci. Adv.* 3 (2017) e1601159.
- [11] W. Ma, H. Kuang, L. Xu, L. Ding, C. Xu, L. Wang, N.A. Kotov, *Nat. Commun.* 4 (2013) 2689.
- [12] A.B. Chinen, C.M. Guan, J.R. Ferrer, S.N. Barnaby, T.J. Merkel, C.A. Mirkin, *Chem. Rev.* 115 (2015) 10530–10574.
- [13] W. Ma, M. Sun, P. Fu, S. Li, L. Xu, H. Kuang, C. Xu, *Adv. Mater.* 29 (2017) 1703410.
- [14] X. Wu, L. Xu, L. Liu, W. Ma, H. Yin, H. Kuang, L. Wang, C. Xu, N.A. Kotov, *J. Am. Chem. Soc.* 135 (2013) 18629–18636.
- [15] Z.Y. Bao, W. Zhang, Y.-L. Zhang, J. He, J. Dai, C.-T. Yeung, G.-L. Law, D.Y. Lei, *Angew. Chem. Int. Ed.* 56 (2017) 1283–1288.
- [16] Y. Duan, X. Liu, L. Han, S. Asahina, D. Xu, Y. Cao, Y. Yao, S. Che, *J. Am. Chem. Soc.* 136 (2014) 7193–7196.
- [17] B.P. Bloom, V. Kiran, V. Varade, R. Naaman, D.H. Waldeck, *Nano Lett.* 16 (2016) 4583–4589.
- [18] P.C. Chen, X.L. Liu, J.L. Hedrick, Z. Xie, S.Z. Wang, Q.Y. Lin, M.C. Hersam, V.P. Dravid, C.A. Mirkin, *Science* 352 (2016) 1565–1569.
- [19] D. Liu, X. Xu, Y. Du, X. Qin, Y. Zhang, C. Ma, S. Wen, W. Ren, E.M. Goldys, J.A. Piper, S. Dou, X. Liu, D. Jin, *Nat. Commun.* 7 (2016) 10254.
- [20] X. Wang, J. Feng, Y. Bai, Q. Zhang, Y. Yin, *Chem. Rev.* 116 (2016) 10983–11060.
- [21] H. Lin, S. Lee, L. Sun, M. Spellings, M. Engel, S.C. Glotzer, C.A. Mirkin, *Science* 355 (2017) 931–935.
- [22] C. Shen, X. Lan, C. Zhu, W. Zhang, L. Wang, Q. Wang, *Adv. Mater.* 29 (2017) 1606533.
- [23] G. González-Rubio, P. Díaz-Núñez, A. Rivera, A. Prada, G. Tardajos, J. González-Izquierdo, L. Báñares, P. Llobmart, L.G. Macdowell, M. Alcolea Palafox, L.M. Liz-Marzán, O. Peña-Rodríguez, A. Guerrero-Martínez, *Science* 358 (2017) 640–644.
- [24] T. Udayabhaskararao, T. Altantzis, L. Houben, M. Coronado-Puchau, J. Langer, R. Popovitz-Biro, L.M. Liz-Marzán, L. Vuković, P. Král, S. Bals, R. Klajn, *Science* 358 (2017) 514–518.
- [25] J.K. Choi, B.E. Haynie, U. Tohgha, L. Pap, K.W. Elliott, B.M. Leonard, S.V. Dzyuba, K. Varga, J. Kubelka, M. Balaz, *ACS Nano* 10 (2016) 3809–3815.
- [26] T. Nakashima, Y. Kobayashi, T. Kawai, *J. Am. Chem. Soc.* 131 (2009) 10342–10345.
- [27] B.P. Bloom, B.M. Graff, S. Ghosh, D.N. Beratan, D.H. Waldeck, *J. Am. Chem. Soc.* 139 (2017) 9038–9043.
- [28] N. Shukla, M.A. Bartel, A.J. Gellman, *J. Am. Chem. Soc.* 132 (2010) 8575–8580.
- [29] Y. Zhu, H. Wang, K. Wan, J. Guo, C. He, Y. Yu, L. Zhao, Y. Zhang, J. Lv, L. Shi, R. Jin, X. Zhang, X. Shi, Z. Tang, *Angew. Chem. Int. Ed.* 57 (2018) 9059–9063.
- [30] M. Naito, K. Iwahori, A. Miura, M. Yamane, I. Yamashita, *Angew. Chem. Int. Ed.* 49 (2010) 7006–7009.
- [31] A.A. Maksimov, I.I. Tartakovskii, E.V. Filatov, S.V. Lobanov, N.A. Gippius, S.G. Tikhodeev, C. Schneider, M. Kamp, S. Maier, S. Höfling, V.D. Kulakovskii, *Phys. Rev. B* 89 (2014) 045316.
- [32] S. Huo, P. Duan, T. Jiao, Q. Peng, M. Liu, *Angew. Chem. Int. Ed.* 56 (2017) 12174–12178.
- [33] U. Tohgha, K.K. Deol, A.G. Porter, S.G. Bartko, J.K. Choi, B.M. Leonard, K. Varga, J. Kubelka, G. Müller, M. Balaz, *ACS Nano* 7 (2013) 11094–11102.
- [34] K. Michaeli, N. Kantor-Uriel, R. Naaman, D.H. Waldeck, *Chem. Soc. Rev.* 45 (2016) 6478–6487.
- [35] M. Karen, V. Vaibhav, N. Ron, H.W. David, *J. Phys. Condens. Matter* 29 (2017) 103002.
- [36] X. Gao, X. Zhang, K. Deng, B. Han, L. Zhao, M. Wu, L. Shi, J. Lv, Z. Tang, *J. Am. Chem. Soc.* 139 (2017) 8734–8739.
- [37] M.V. Mukhina, V.G. Maslov, A.V. Baranov, A.V. Fedorov, A.O. Orlova, F. Purcell-Milton, J. Govan, Y.K. Gun'ko, *Nano Lett.* 15 (2015) 2844–2851.
- [38] J. Cheng, J. Hao, H. Liu, J. Li, J. Li, X. Zhu, X. Lin, K. Wang, T. He, *ACS Nano* 12 (2018) 5341–5350.
- [39] A. Ben-Moshe, A. Teitelboim, D. Oron, G. Markovich, *Nano Lett.* 16 (2016) 7467–7473.
- [40] A. Bobrovsky, K. Mochalov, V. Oleinikov, A. Sukhanova, A. Prudnikau, M. Artemyev, V. Shibaev, I. Nabiev, *Adv. Mater.* 24 (2012) 6216–6222.
- [41] F. Qiu, Z. Han, J.J. Peterson, M.Y. Odoi, K.L. Sowers, T.D. Krauss, *Nano Lett.* 16 (2016) 5347–5352.
- [42] U. Tohgha, K. Varga, M. Balaz, *Chem. Commun.* 49 (2013) 1844–1846.
- [43] W. Mtangi, V. Kiran, C. Fontanesi, R. Naaman, *J. Phys. Chem. Lett.* 6 (2015) 4916–4922.
- [44] R. Shi, Y. Cao, Y. Bao, Y. Zhao, G.I.N. Waterhouse, Z. Fang, L.-Z. Wu, C.-H. Tung, Y. Yin, T. Zhang, *Adv. Mater.* 29 (2017) 1700803.
- [45] K. Wu, Z. Chen, H. Lv, H. Zhu, C.L. Hill, T. Lian, *J. Am. Chem. Soc.* 136 (2014) 7708–7716.
- [46] K.A. Brown, M.B. Wilker, M. Boehm, G. Dukovic, P.W. King, *J. Am. Chem. Soc.* 134 (2012) 5627–5636.
- [47] T. Simon, M.T. Carlson, J.K. Stolarczyk, J. Feldmann, *ACS Energy Lett.* 1 (2016) 1137–1142.
- [48] Y. Ben-Shahar, F. Scotognella, I. Kriegel, L. Moretti, G. Cerullo, E. Rabani, U. Banin, *Nat. Commun.* 7 (2016) 10413.
- [49] T.-T. Zhuang, Y. Liu, M. Sun, S.-L. Jiang, M.-W. Zhang, X.-C. Wang, Q. Zhang, J. Jiang, S.-H. Yu, *Angew. Chem. Int. Ed.* 54 (2015) 11495–11500.
- [50] T.-T. Zhuang, Y. Liu, Y. Li, Y. Zhao, L. Wu, J. Jiang, S.-H. Yu, *Angew. Chem. Int. Ed.* 55 (2016) 6396–6400.
- [51] T. Lei, C. Zhou, M.-Y. Huang, L.-M. Zhao, B. Yang, C. Ye, H. Xiao, Q.-Y. Meng, V. Ramamurthy, C.-H. Tung, L.-Z. Wu, *Angew. Chem. Int. Ed.* 56 (2017) 15407–15410.
- [52] Y.-J. Tang, M.-R. Gao, C.-H. Liu, S.-L. Li, H.-L. Jiang, Y.-Q. Lan, M. Han, S.-H. Yu, *Angew. Chem. Int. Ed.* 54 (2015) 12928–12932.
- [53] L.-M. Zhao, Q.-Y. Meng, X.-B. Fan, C. Ye, X.-B. Li, B. Chen, V. Ramamurthy, C.-H. Tung, L.-Z. Wu, *Angew. Chem. Int. Ed.* 56 (2017) 3020–3024.
- [54] Z. Niu, N. Becknell, Y. Yu, D. Kim, C. Chen, N. Kornienko, G.A. Somorjai, P. Yang, *Nat. Mater.* 15 (2016) 1188–1194.
- [55] T.L. Doane, R. Alam, M.M. Maye, *Nanoscale* 7 (2015) 2883–2888.
- [56] K. Manthiram, B.J. Beberwyck, D.V. Talapin, A.P. Alivisatos, *J. Vis. Exp.* (2013) e50731.
- [57] X. Gao, X. Zhang, L. Zhao, P. Huang, B. Han, J. Lv, X. Qiu, S.-H. Wei, Z. Tang, *Nano Lett.* 18 (2018) 6665–6671.
- [58] A. Ben Moshe, D. Szwarcman, G. Markovich, *ACS Nano* 5 (2011) 9034–9043.
- [59] A.S. Baimuratov, I.D. Rukhlenko, Y.K. Gun'ko, A.V. Baranov, A.V. Fedorov, *Nano Lett.* 15 (2015) 1710–1715.
- [60] K. Varga, S. Tannir, B.E. Haynie, B.M. Leonard, S.V. Dzyuba, J. Kubelka, M. Balaz, *ACS Nano* 11 (2017) 9846–9853.
- [61] A. Nadav, S.M. M., *ChemPhysChem* 16 (2015) 2768–2774.
- [62] J. Zylstra, J. Amey, N.J. Miska, L. Pang, C.R. Hine, J. Langer, R.P. Doyle, M.M. Maye, *Langmuir* 27 (2011) 4371–4379.
- [63] Z. Zhu, J. Guo, W. Liu, Z. Li, B. Han, W. Zhang, Z. Tang, *Angew. Chem. Int. Ed.* 125 (2013) 13816–13820.
- [64] W. Yan, L. Xu, C. Xu, W. Ma, H. Kuang, L. Wang, N.A. Kotov, *J. Am. Chem. Soc.* 134 (2012) 15114–15121.
- [65] J.Y. Choi, D. Jeong, S.J. Lee, D.-g. Kang, S.K. Kim, K.M. Nam, H. Song, *Nano Lett.* 17 (2017) 5688–5694.
- [66] T. Simon, N. Bouchonville, M.J. Berr, A. Vaneski, A. Adrović, D. Volbers, R. Wyrwich, M. Döblinger, A.S. Susha, A.L. Rogach, F. Jäckel, J.K. Stolarczyk, J. Feldmann, *Nat. Mater.* 13 (2014) 1013–1018.